JGR Atmospheres

RESEARCH ARTICLE
10.1029/2021JD035238

Bidirectional Recoil Leaders in Upward Lightning Flashes Observed at the Säntis Tower

Antonio Sunjerga[1], Marcos Rubinstein[2], Mohammad Azadifar[1], Amirhossein Mostajabi[1], and Farhad Rachidi[1]

[1]Electromagnetic Compatibility Laboratory, Swiss Federal Institute of Technology (EPFL), Lausanne, Switzerland, [2]University of Applied Sciences of Western Switzerland (HES-SO), Yverdon-les-Bains, Switzerland

Key Points:

- Recoil leaders main source of fast processes in negative lightning
- Recoil leaders initiate in bidirectional manner
- Mixed mode pulses connect directly to structure

Correspondence to:
A. Sunjerga,
antonio.sunjerga@epfl.ch

Citation:
Sunjerga, A., Rubinstein, M., Azadifar, M., Mostajabi, A., & Rachidi, F. (2021). Bidirectional recoil leaders in upward lightning flashes observed at the Säntis Tower. *Journal of Geophysical Research: Atmospheres*, *126*, e2021JD035238. https://doi.org/10.1029/2021JD035238

Received 13 MAY 2021
Accepted 23 AUG 2021

Author Contributions:

Conceptualization: Antonio Sunjerga, Farhad Rachidi
Data curation: Antonio Sunjerga, Mohammad Azadifar, Amirhossein Mostajabi, Farhad Rachidi
Formal analysis: Antonio Sunjerga, Farhad Rachidi
Funding acquisition: Marcos Rubinstein, Farhad Rachidi
Investigation: Antonio Sunjerga, Marcos Rubinstein
Methodology: Antonio Sunjerga, Marcos Rubinstein, Mohammad Azadifar
Project Administration: Marcos Rubinstein, Farhad Rachidi
Software: Antonio Sunjerga
Supervision: Marcos Rubinstein, Farhad Rachidi
Validation: Antonio Sunjerga
Visualization: Antonio Sunjerga
Writing – original draft: Antonio Sunjerga, Marcos Rubinstein, Farhad Rachidi

Abstract We report the observation of three negative upward flashes recorded by a high-speed camera at the Säntis Tower during the Summer of 2019. The camera was operating at 10,000 fps and an exposure time of 99 μs. Simultaneous measurements of the lightning current were obtained for all three flashes. The close electric field was measured for one of the observed flashes, which was analyzed in detail. In this flash, we observed 50 recoil leaders developing in the decayed channel with speeds characteristic of dart leader processes. Out of the 50 recoil leaders, 45 ended up as attempted leaders, three developed into M-component-type ICC (initial continuous current) processes, and two into return strokes. This study reveals that depending on the spatial and temporal properties of electric field in the area of the event and the main channel condition, recoil leaders can develop into different processes in upward negative lightning flashes such as attempted leaders, M-components, M-component-type ICC events, mixed mode pulses, or return strokes. We observed M-component-type ICC events with junction heights as low as 137 m, while all of the observed mixed mode pulses seemed to attach directly to the structure. Bidirectional propagation of the recoil leader was also observed.

1. Introduction

Upward lightning typically initiates from tall-grounded structures (greater than about 100 m) or from moderately tall structures (tens of meters) located in an elevated terrain. Understanding the mechanism of initiation of upward lightning is an important research topic because this type of lightning is predominant for tall structures such as telecommunications towers and wind turbines.

Several tall structures have been instrumented for lightning observations over the world (e.g., the Gaisberg, Peissenberg, Säntis, Skytree and CN towers). Measurements on these towers have led to reports on lightning current measurements (e.g., Diendorfer et al., 2009; Heidler et al., 2013; Hussein et al., 1995; and Romero et al., 2013; and Shinodo et al., 2014), electric field measurements (e.g., Azadifar et al., 2016; Heidler et al., 2013; and Zhou et al., 2015), and high-speed camera (HSC) observations (e.g., Mazur et al., 2013; Qie et al., 2017).

Different terms have been used to identify different processes in the lightning discharge, which are briefly summarized in what follows. In upward negative and downward negative lightning, one can observe subsequent return strokes (RSs) preceded by dart leaders (DLs) that propagate from the upper parts of the channel to the ground termination. If the DL stops before reaching the ground, the process is called an attempted leader (AL). Although no current is observed at the bottom of the channel in ALs, they do produce electric field changes that are known as K changes or K-events (Kitagawa & Brook, 1960). Note that a K-event can occur both in cloud-to-ground and in cloud lightning. M components occur when a floating leader connects to the upper part of the conducting channel created by the previous RS. Additionally, mixed mode (MM) pulses and M-component-type initial continuous current (ICC) pulses occur only in upward lightning (He et al., 2018; Zhou et al., 2015). These two types of pulses exhibit similarities, respectively, with the main pulse in the RS process and with the pulses that characterize the M component process, the main difference being that MM and M-component-type ICC (M-ICC) pulses occur during the ICC phase in upward negative lightning. Zhou et al. (2015) defined "mixed mode of charge transfer to ground" as an occurrence of RS like process in one of the branches of the UPL, while the channel is still conducting the ICC current. The corresponding pulse superimposed on the ICC current is called an MM pulse.

Writing – review & editing: Antonio Sunjerga, Marcos Rubinstein, Mohammad Azadifar, Amirhossein Mostajabi, Farhad Rachidi

Using an interferometer system, Shao et al. (1995) showed that RSs, M components, and ALs can be considered to belong to a single class of processes that start some distance beyond the flash origin (therefore extending the channel) and travel toward the main channel. The only difference between the M components and the RSs is that, in the case of RSs, the floating leader connects to a decayed main channel and reaches the ground (DL), while in M components, the floating leader connects to a conducting channel carrying a continuing or continuous current. The third and last member of the class, ALs, occur in the same manner as DLs but they stop before reaching the ground (Cooray, 2014, page 121). The observations of Shao et al. (1995) were confirmed by Mazur (2002), Mazur and Ruhnke (2011), and Mazur et al. (2013), who also attributed the same origin for these different phenomena further observing that floating leader was recoil leader (RL).

RLs are self-propagating discharges, moving along a previously ionized channel (Mazur, 2002) that occur in decayed positive leaders (as observed by means of lightning mapping arrays). They are thought to be the cause of K-changes (Mazur et al., 2013). Saba et al. (2008) made the first observation of recoil leaders with a high-speed camera.

It was suggested and observed (Mazur, 2002; Mazur & Ruhnke, 2011; Mazur et al., 2013) that these RLs occur in a bidirectional manner similar to observations in in-cloud lightning discharges and downward stepped leaders (Kasemir, 1950; Mazur & Ruhnke, 1993). The negative end of the RL travels toward the origin, which can be either a grounded structure or a branching point while the positive end propagates in the opposite direction outward and possibly extending the channel through virgin air propagation (Warner et al., 2016). Mazur (2002) argued that unidirectional propagation observed by lightning mapping array (LMA) systems is due to the fact that the negative leader radiates much more in the relevant frequency range of LMA systems (VHF) than the positive, and these systems are not able to measure both positive and negative leaders at the same time.

In later studies, a series of HSC observations of bidirectional RLs have been reported. Bidirectional RLs have been observed by Kotovsky et al. (2019) in rocket-triggered lightning during an M component event. They have also been observed to occur in ALs in both tower-initiated lightning (Jiang et al., 2014) and rocket-triggered lightning (Qie et al., 2017). Wu et al. (2019) and Zhu et al. (2019) observed bidirectional propagation in the DL phase of a tower-initiated upward flash preceding the RS phase. Warner et al. (2012) reported one of the biggest HSC data sets of upward lightning recording 81 upward flashes during a period of 6 years from 10 different towers. Bidirectional propagation was unambiguously observed both in RLs connecting to the conducting main channel and directly to the towers. Unfortunately, due to the lack of current measurements, it is not possible to distinguish MM and M-ICC pulses. Furthermore, the authors did not report that any of the RLs reaching either the conducting main channel or the tower tip occurred while some other upward branch was active suggesting that all RLs connecting to the conducting main channel are either M-ICC or M-component-type pulses. Zhou et al., 2015 using HSC observations and current measurements observed a difference in the junction height between M-ICC or M-component-type pulses. However, their relatively high exposure time of 2 ms did not allow to observe the RL mechanism.

Using an interferometer, Yoshida et al. (2012) observed that AL can be started both by RLs in the decayed branches and by virgin air breakdown (propagating toward the pre-existing channel). Later, Warner et al. (2016) observed that AL initiated in virgin air starts in a similar way as AL caused by RL with bidirectional propagation.

In this paper, we report simultaneous measurements of current, close electric field and HSC images for three upward negative flashes initiated from the Säntis Tower in Switzerland. The close-range electric field was only measured in one of the flashes, which we analyze in detail. We observed parts of the upward positive leader (UPL) propagation during the ICC phase that reveal different processes that started as RLs. The aim of the present study is to identify and analyze the role of RLs in upward negative flashes using HSC observations, simultaneously with lightning current and electric field measurements.

The rest of this paper is organized as follows. In Section 2, we briefly describe the Säntis Tower facility and the measurement sensors. The obtained data for the considered flashes are presented in Section 3. Section 4 is devoted to the analysis of the observed RLs and their role in the various processes in upward negative

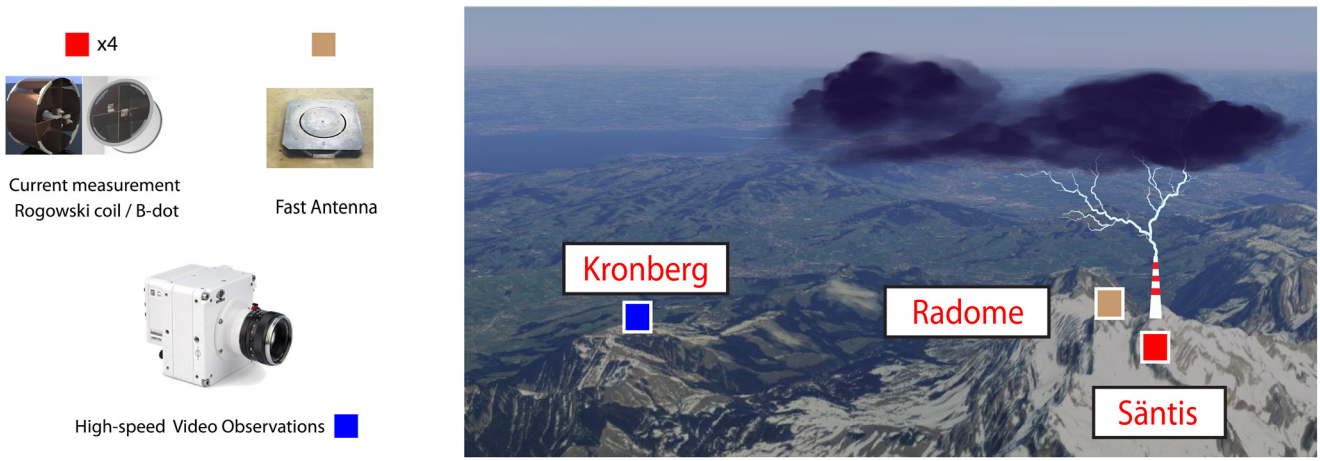

Figure 1. Sketch of location of the tower, close electric field station and high-speed camera (HSC). Not to scale.

flashes. The observed bidirectional propagation in three RLs is discussed in Section 5. The paper ends with a general discussion (Section 6) and concluding remarks (Section 7).

2. Measurement Setup

The 124-m tall Säntis Tower, located in the Northeastern part of Switzerland, is by far the most frequently struck structure in Switzerland (Romero et al., 2012). The tower has been instrumented for current measurements since May 2010. Throughout the years, the station has been upgraded and enhanced with electromagnetic field and optical measurement systems. More details about the station and its instrumentation can be found in (Azadifar et al., 2014; Romero et al., 2010, 2012). Locations of the equipment used in this study can be seen in Figure 1.

A wideband Mélopée electric field sensor, purchased from the now-defunct company Thomson-CSF, was installed and connected to a digitizer with 5 MS/s sampling rate during the Summer of 2018 (some information on the sensor can be found in Li et al., 2016). The sensor was installed about 23 m away from the tower in the radome (structural, weatherproof enclosure transparent for electromagnetic waves) building next to the tower used commercially for broadcasting signals in different bandwidths. The estimated time constant of the sensor is about 20 μs, which as explained later in Section 3, was compensated to 400 μs. The electric field antenna does not have GPS time synchronization and its output was manually aligned with the current measurements. Note that the electric field measurements are to some extent affected by the shadowing effect of the tower (Smorgonskiy et al., 2015). An evaluation of this effect is beyond the scope of this paper.

A Phantom VEO 710L HSC is installed on the Kronberg mountain about 5 km away from the tower. The camera can record up to 1,000,000 FPS at its lowest resolution of 8 × 8 pixels. To have a wider view of 512 × 512 pixels, the number of frames per second has been reduced to 10,000. These pixels are distributed over a view of about 1,700 m by 1,700 m in the plane of the tower, perpendicular to the view with a resolution of about 3.4 m per pixel. The camera records during a 3-s time window with a pretrigger delay of 1.5 s. A GPS time stamp is provided by an Acutime 360 Multi-GNSS Smart Antenna. However, it was not operational at the time of the observed flashes, so that the time synchronization was obtained manually.

During 2019, only three negative flashes could be observed with the HSC, all of the other flashes to the tower having been obscured by the clouds. The first flash, referred to as Flash #1 in this work, occurred on July 18, 2019 at 17:58 UTC. The second, Flash #2, occurred the day after, on July 19, 2019 at 21:01 UTC, followed about 4 min later by the third, Flash #3, at 21:05 UTC. For all three flashes, the system recorded the current. The electric field was obtained only for Flash #3, which will be analyzed in detail in this study.

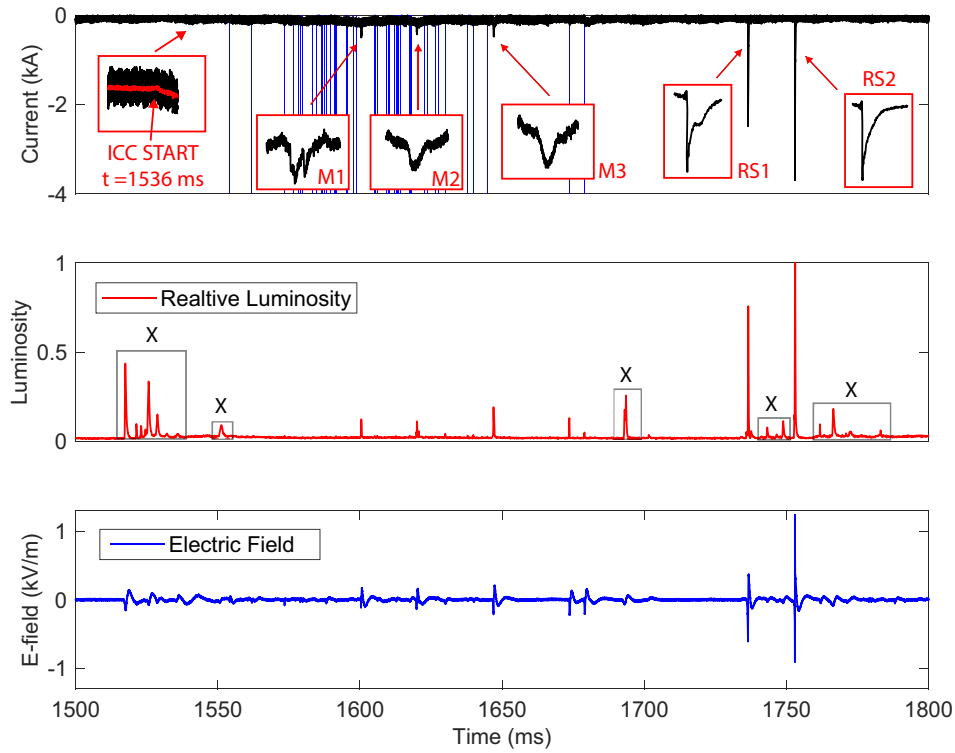

Figure 2. Measured waveforms for the duration of the whole Flash#3. Top: Current waveform. Blue vertical lines indicate attempted leaders (ALs) observed on the high-speed camera (HSC). Middle: Relative luminosity of each frame with distant events shown in gray boxes and marked with the letter X. Bottom: Electric field measured at a distance of 23 m with the fast antenna (atmospheric sign convention). Note that the start of the initial continuous current (ICC), marked with the red line in the top subplot, was determined by filtering the current waveform (lowpass 1 kHz and band-stop 50 Hz filter).

3. Summary of Obtained Data for Flash #3

Figure 2 presents the simultaneously measured waveforms for Flash #3. The time is relative to the start of the record. The upper plot presents the current waveform measured with the Rogowski coil at 24 m above the tower base, the middle plot presents the sum of luminosity of all pixels in relative units versus time measured by the camera and, finally, in the bottom plot we can observe the electric field measured by the fast antenna 23 m away from the tower. As mentioned in Section 2, the amplitude of the electric field measurements is affected by the shadowing effect of the nearby tower (Smorgonskiy et al., 2015).

During the flash, we recorded 50 RLs. Forty five out of the 50 ended up as ALs as they did not reach the ground, three developed into M-ICC processes, and two into RSs. The times of initiation of ALs are indicated with blue lines in the top subplot of Figure 2. The luminosity of the channel is shown in the middle subplot where events that are not directly related to the tower flash (either cloud or nearby lightning) are framed in a gray box and marked with the letter X.

Figure 3 presents selected frames from the Flash #3 and simultaneous measurements of the current and the electric field. In the electric field plots, the black line represents original waveforms obtained from the fast antenna with a 20 μs decay time constant. Since the decay time is in the same order of magnitude of the recorded events, we also present, in red, the waveform compensated to a decay time constant of 400 μs, centered at the timestamp of each frame, based on the method proposed by Rubinstein et al. (2012). Note that the vertical scale in the compensated electric field waveforms is bigger than the scale in the uncompensated ones; as a result, the fast changes are less discernible. The red shaded time intervals in the field plots are 160 μs wide and they represent a 99 μs exposure of each frame and an extra 61 μs estimated uncertainty due to the manual time synchronization. The red vertical segment in the bottom of the frames represents

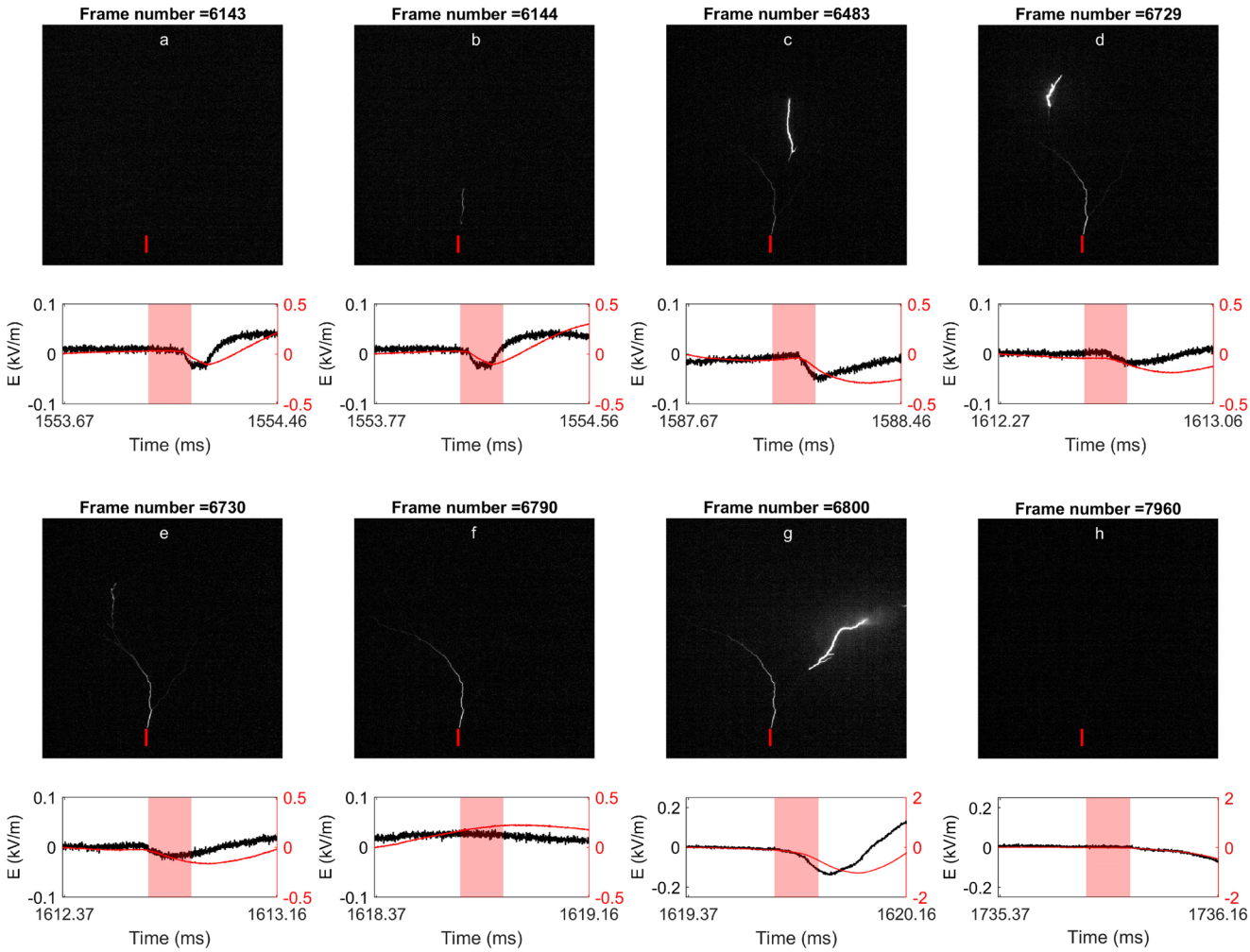

Figure 3. Selected high-speed camera (HSC) frames for the upward negative Flash #3 (top panels). The associated electric field changes at 23 m are shown in the respective bottom panels. The red shaded time intervals in the field plots are 160 μs wide and they represent a 99 μs exposure of each frame and an extra 61 μs estimated uncertainty due to the manual time synchronization. The red vertical segment in the bottom of the frames represent the 124-m tall Säntis Tower. The black line represents waveforms obtained from the fast antenna with a 20 μs decay time and the red line is the waveform compensated to a decay time of 400 μs centered at the timestamp of each frame based on the method proposed by Rubinstein et al. (2012).

the 124-m tall Säntis Tower. The above description is valid for all the following figures presenting multiple HSC frames.

The ICC current started somewhere after the time 1,536 ms. A slight intensification of the luminosity, probably due to nearby lightning, was observed at about 1,551 ms. The first RL was recorded at time 1,554 ms (see Figure 3b), before which (Figure 3a) we were not able to observe the propagation of the upward positive leader due to low luminosity. Only after the first RL, was the UPL channel heated, making it visible in subsequent frames. At later times, the UPL channel was extending and, since it was heated by RLs, the ICC current and M-component type processes, some part of it remained continuously visible as shown in Figures 3c–3h. Most of the RLs lasted less than the duration of one frame (99 μs). In Figure 3g, we can observe the start of an M-ICC event (M1) illuminating the channel on the right side of the frame.

The ICC channel decayed at about 1,736 ms (as shown in Figure 3h) when the RS1 (see Figure 2) was initiated. At that time, the first subsequent RS occurred and its channel decayed about 15 ms later. The RS1 channel was barely visible when the following subsequent RS2 (see Figure 2) was initiated. About 10 ms later, the channel was no longer visible and some distant activity followed. In Figure 4, we present the time-integrated image for the duration of the whole flash. The first branching of the channel occurs at a

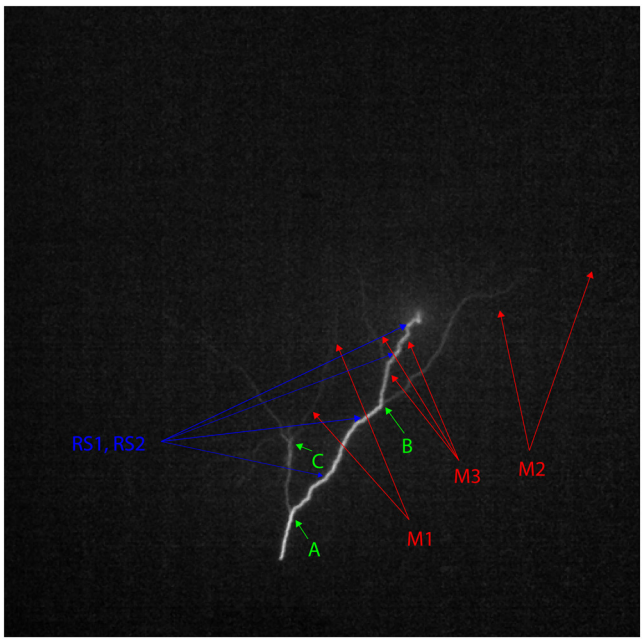

Figure 4. Time integrated image for the duration of whole Flash#3 (Altitudes of branching points: A 137 m, B 422 m, and C 325 m). Channels that were involved in each one of the RSs (RS1 and RS2) and M components (M1, M2, and M3) are pointed to with arrows.

height of about 137 m above the tower tip (labeled A in Figure 4). Note that, as previously observed in the literature (Krehbiel et al., 1979), for each subsequent stroke, the lightning leaders will propagate further away than the preceding leader. In this specific case, since the flash had only two RSs, most of the processes were located in the view of the camera (about 1,700 × 1,700 m). A similar behavior was observed at the Säntis Tower by LMA observations (Sunjerga et al., 2020).

4. Recoil Leaders

In this section, we discuss the RLs observed in Flash #3. These RLs can be classified as different transient events: (a) ALs, (b) M-ICC pulses, or (c) DLs, based on whether they reached the ground or if they attached to the conducting channel. We have also observed classical M components and MM pulses in two other flashes data provided in the supplementary material in Sunjerga, Rachidi, and Rubinstein (2021) that are not analyzed here in detail. It is worth noting that, in the literature, these different transient events could be either due to a RL propagating along a previously ionized channel (e.g., Mazur et al., 2013) or due to a newly ionized channel (Warner et al., 2016; Yoshida et al., 2012); however, all of the events observed in our three flashes were due to RLs. We classify them as RLs based on the fact that they all develop with speeds characteristic of propagation along a previously ionized channel while, additionally, for most of them, we can observe from camera frames that they propagate indeed along a previously ionized channel. It is worth noting that our measurements could be somehow biased by the fact that, in some cases, leaders extend out of the camera view or they are obscured by the clouds.

4.1. Attempted Leaders

Figure 5 presents four representative samples of ALs that occurred during the flash by order of occurrence. The associated electric field changes at 23 m are also shown. We can observe that the electric field is strongest in the first event shown in Figure 5a since the leader is close to the tower. The leaders in Figures 5a and 5c are much brighter compared to those in Figures 5b and 5d.

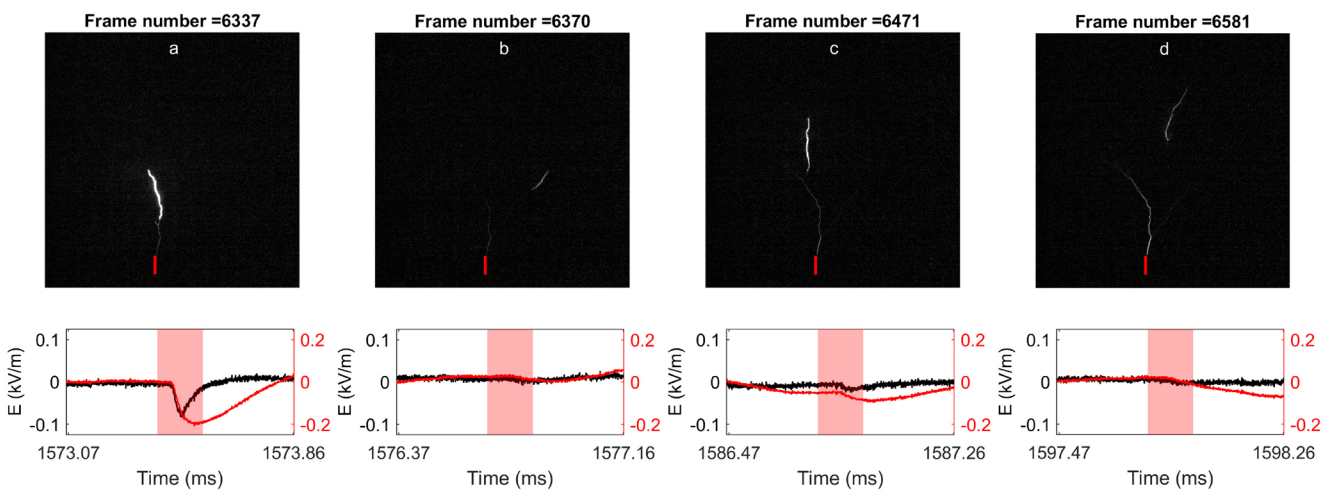

Figure 5. Video frames of representative samples of attempted leaders (ALs) and the electric field at 23 m. See more detailed description of subplots in the caption of Figure 3.

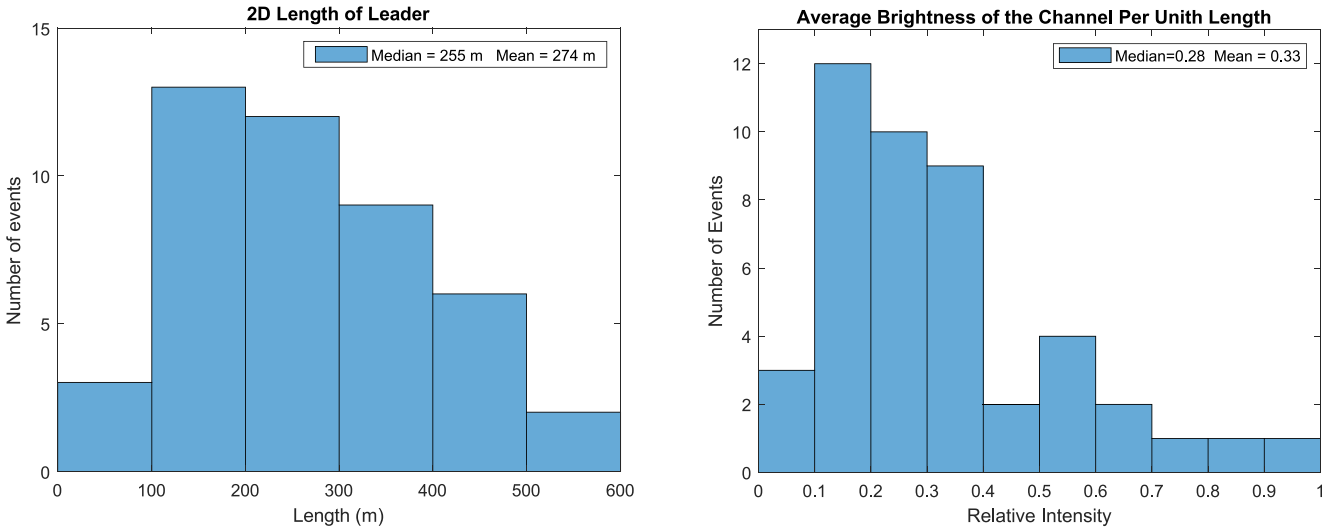

Figure 6. Attempted leaders (ALs) histograms. (a) Length of the leader (b) Average brightness of the channel per unit length.

Most of the ALs were visible only in one frame and the 2D-inferred length was typically in the range of 100–500 m as shown in Figure 6a. The propagation speed of the leaders could not be accurately estimated because of the limited number of frames. The observations allow only to conclude that the speed is at least higher than 10^6 m/s, probably in the range of about 10^7 m/s, which is typically the speed of leaders reactivating decayed channels (e.g., Qie et al., 2017). The median 2D length of the ALs was about 255 m. In the later stages of the flash, five of the ALs were characterized by longer lengths than reported here since the leaders extended beyond the camera view. The reported lengths may be further underestimated because of the possible clouds obscuring the view.

Figure 6b presents the histogram of average light brightness per unit length of each event. The average brightness per unit length is calculated by taking, for each horizontal line containing the leader, the brightest pixel. We then averaged the pixel intensities along the 2D leader length and divided it by the 2D leader length. The calculated average brightness per unit length shows a wide spread: the brightest observed leaders are about 14 times brighter than the darkest ones.

The Pearson correlation coefficient ($R = 0.5025$) with statistical significance ($P = 0.0004$) indicates some positive correlation between the length of the leader and the average brightness per unit length. The longer the leader, the brighter it is. The length of the RL as well as its brightness could depend on multiple parameters such as the conditions in the decayed channel, and the spatial and temporal distribution of the total electric field.

4.2. M-Component-Type ICC Pulses

In this section, we discuss three M-ICC events. All three were characterized by a relatively low-peak current (about 500 A). The first event is shown in Figure 7. It started with two RLs as seen in Figure 7c, one of them reached in Figure 7d the branching point C (see Figure 4). The total electric field in this case is the sum of the contributions from the downward propagating negative charge due to the first RL and, once it connects to the channel, from the M-ICC pulse. The stationary point of the compensated electric field (shown with a red arrow in Figure 7e) occurs when the contribution in the electric field change at location of measurements of the positive charge supplied by the tower to the channel becomes higher than the contribution due to the negative charge flowing downward from the charge sources in the cloud. After the RL attached the channel and initiated an M-ICC event, the luminosity intensified across the whole channel (Figure 7e), presumably due to the M-ICC pulse propagation. Another RL connected to the visible channel in the upper part of Figure 7e that caused another subpeak and another M-ICC pulse in the current waveform.

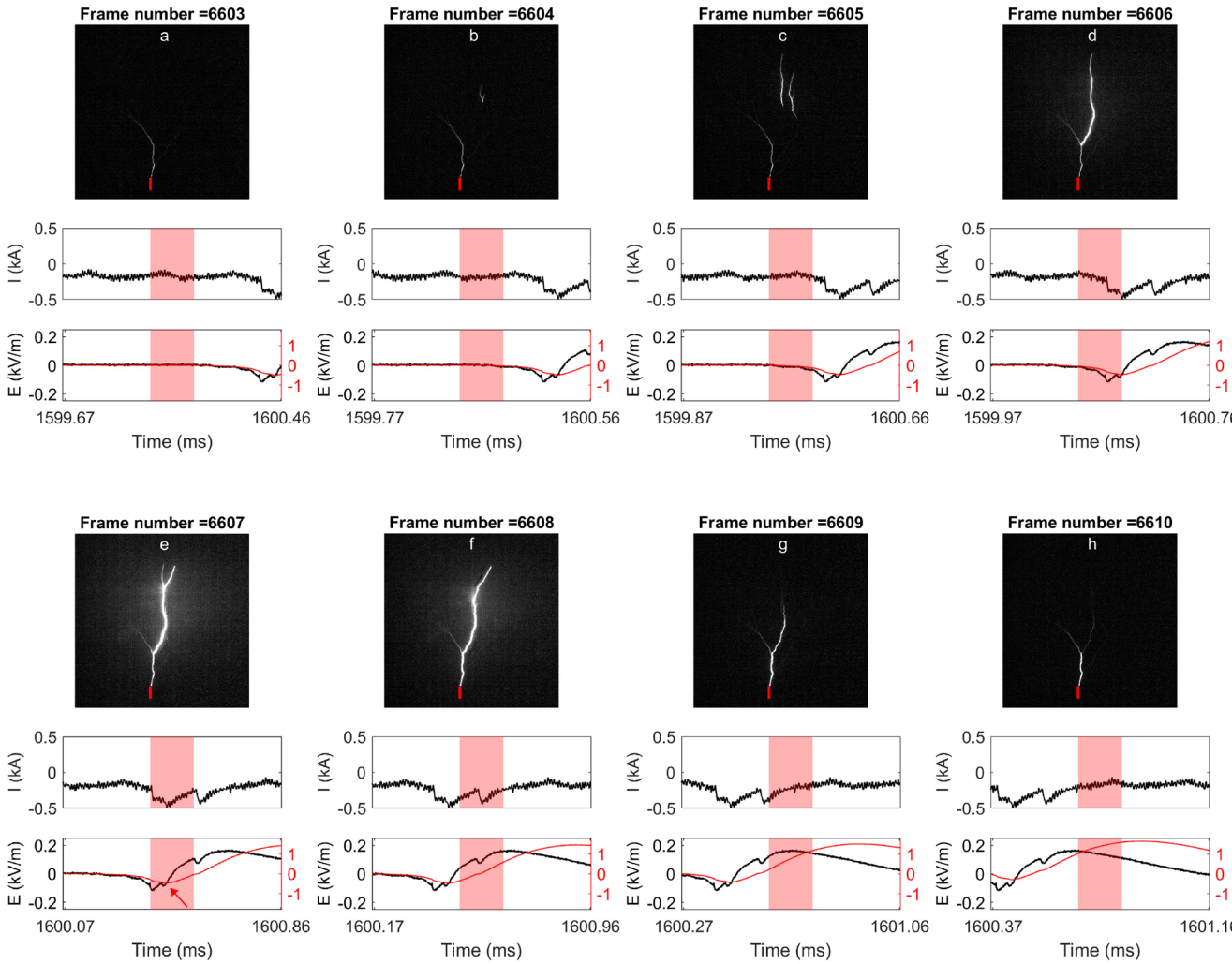

Figure 7. The first M-initial continuous current (ICC) pulse in Flash #3. In parts (a) through (h), frames from the HSC are shown at the top, the current waveform plot in the middle and the electric field plot at the bottom. See more detailed description of subplots in the caption of Figure 3.

The second M-ICC event, shown in Figure 8, occurred about 20 ms later. The initiation of the RL is discernible on the right-hand side of the video frame in Figure 8b. The RL extended further in Figure 8c. In the next frame (Figure 8d), the RL was not propagating further, even though the luminosity of the decayed channel just below the RL slightly increased (it is possible that the propagation occurred during the last few microseconds of the exposure time of this frame). In the following frame, Figure 8e, the RL attached to the channel and a current was measured at the tower.

The third and last M-ICC event occurred about 25 ms after the second one. The start of the RL can be observed as a bright spot in Figure 9b. It further extended in the next frame (Figure 9c) and connected to the branching point B as shown in Figure 9d. The 2D speed of the leader between the frames in Figures 9b and Figure 9(c) is estimated to be 1.8×10^6 m/s.

In these three events, we can observe the following mechanism. First, due to the electric field, the RL is initiated in the decayed channel creating negative charge density in the lower part of the leader. When this RL connects to the conducting channel, the M-ICC event is initiated, and it propagates down the conducting channel. Once the M-ICC event reaches the tower tip, the whole channel becomes highly conductive and a pulse superimposed on the ICC current can be observed at the tower. The low current peaks in these three cases can be due to the small length of these RLs (Cooray et al., 2020). There is no clear relation between the current risetime (about 60 μs for all the three events) and the junction height (137, 325, and 422 m).

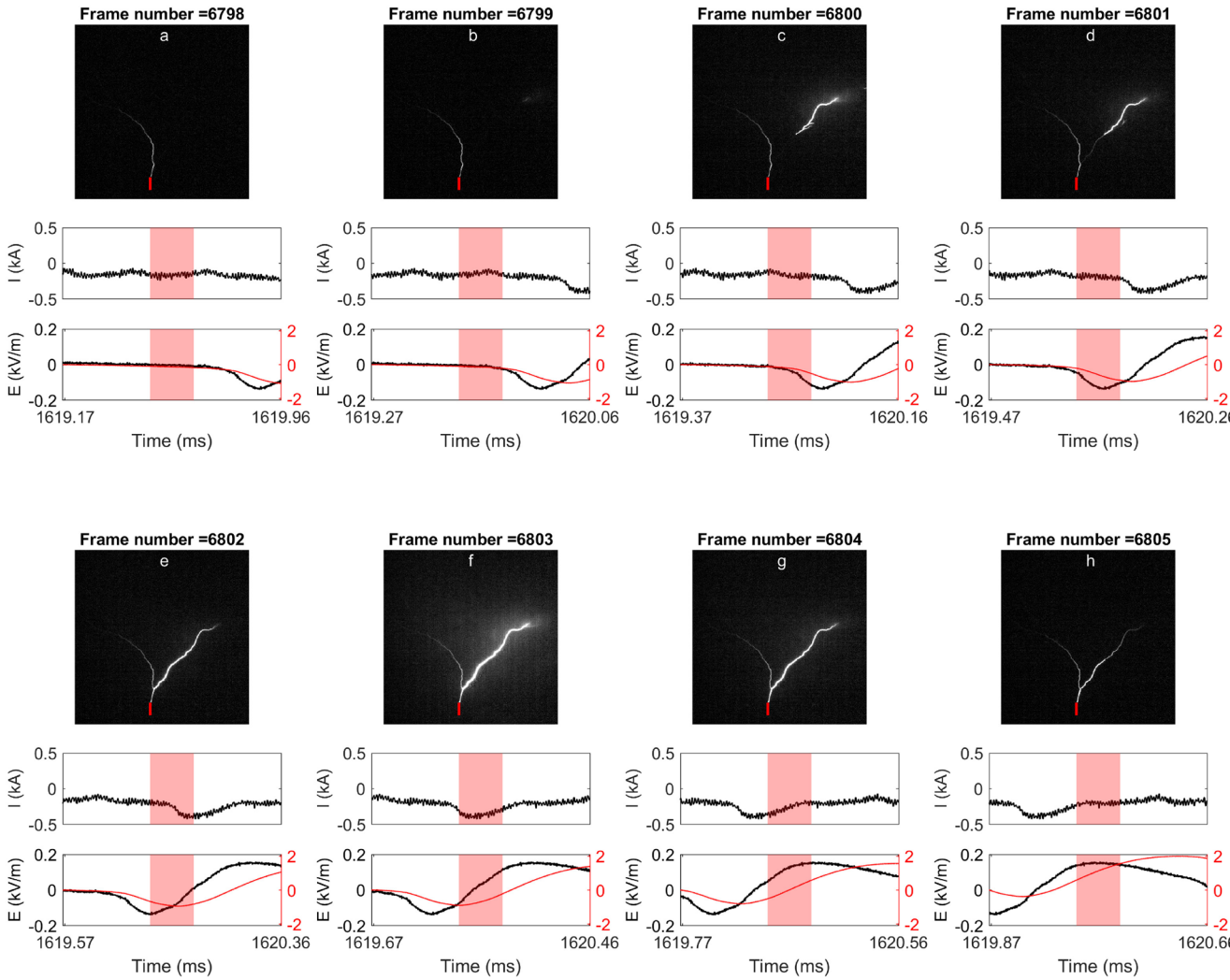

Figure 8. The second M-initial continuous current (ICC) pulse. See description of subplots in the captions of Figures 3 and 7.

Zhou et al. (2015) observed that: "When the connection point is a kilometer or more above the tower top (inside the cloud), the M-component mode takes place, and if it is very close to the tower top (say, 10 m), the mixed mode (involving two channels below the cloud base) is likely." Note that in the case of the Säntis and Gaisberg towers (Zhou et al., 2015), due to the high altitude above sea level of the mountains on which the towers are constructed, thunderclouds are frequently very close to the structure.

All three M-ICC events observed in Flash#3 connected to the channel at a relatively low altitude of a few hundred meters, in one case less than 150 m above the tower tip (137 m), providing evidence that the junction point of M-ICC events can be significantly lower than the 1-km threshold suggested by Zhou et al. (2015).

On the other hand, in agreement with Zhou et al. (2015), we observed in Flash #2 (data in supplementary material, Sunjerga, Rachidi, & Rubinstein, 2021) that RLs associated with MM pulses connected either directly to the structure top, or to the conducting channel only a few meters above the tower tip (the resolution of the observation system does not allow a clear distinction).

Also, it is worth noting that, in the three observed cases, we clearly see that the channel branch above the junction point is much brighter and thicker (similar to RSs, but less bright) than the lower part of the channel (below the junction point), which is consistent with the M-component model proposed by Azadifar

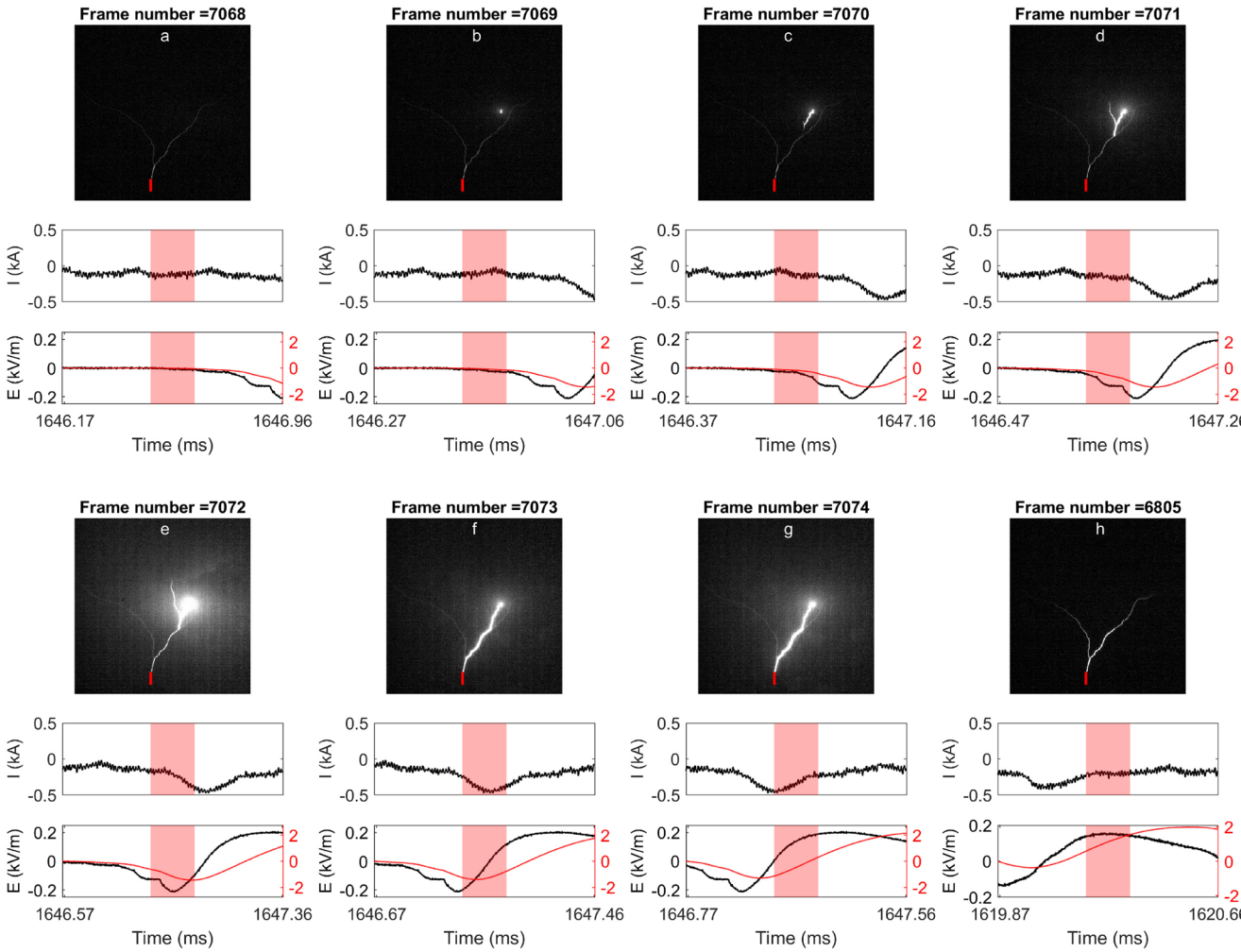

Figure 9. The third M-initial continuous current (ICC) pulse. See description of subplots in the captions of Figures 3 and 7.

et al. (2019). Note that three observed events have relatively low current peaks, which could explain the lower brightness.

4.3. Dart Leaders

In this section, we discuss two RSs belonging to Flash #3, which occurred after the extinction of the ICC. The observed images, current and electric field waveforms for the first are shown in Figure 10. Figure 10a shows the start of a RL. Since it was relatively slow, we were able to estimate the average 2D speed for Figure 10b frame to be 6.55×10^6 m/s. The peak value of the current is only about 2.5 kA with a risetime of about 3.7 μs. The characteristic asymmetrical V-shape (Rubinstein et al., 1995) can be seen in the uncompensated waveform, the bottom of which corresponds to the start of the RS.

The second RS was initiated about 15 ms after the previous one and it is shown in Figure 11. In Figure 11a, we can observe some in-cloud activity, which was not sensed by the E-field sensor. In the following frames, the RL reached the tower, initiating the RS. Distant activity can still be observed in Figure 11e–11f. The peak value of the current is about 3.7 kA with a risetime of about 4 μs.

In both cases, the initiation point is stationary and there is no observed upward extension even after the RS phase. However, one can again observe in both cases (see Figures 10d and 11e) that in the area around the initiation point, the light is highly dispersed, presumably indicating the presence of clouds.

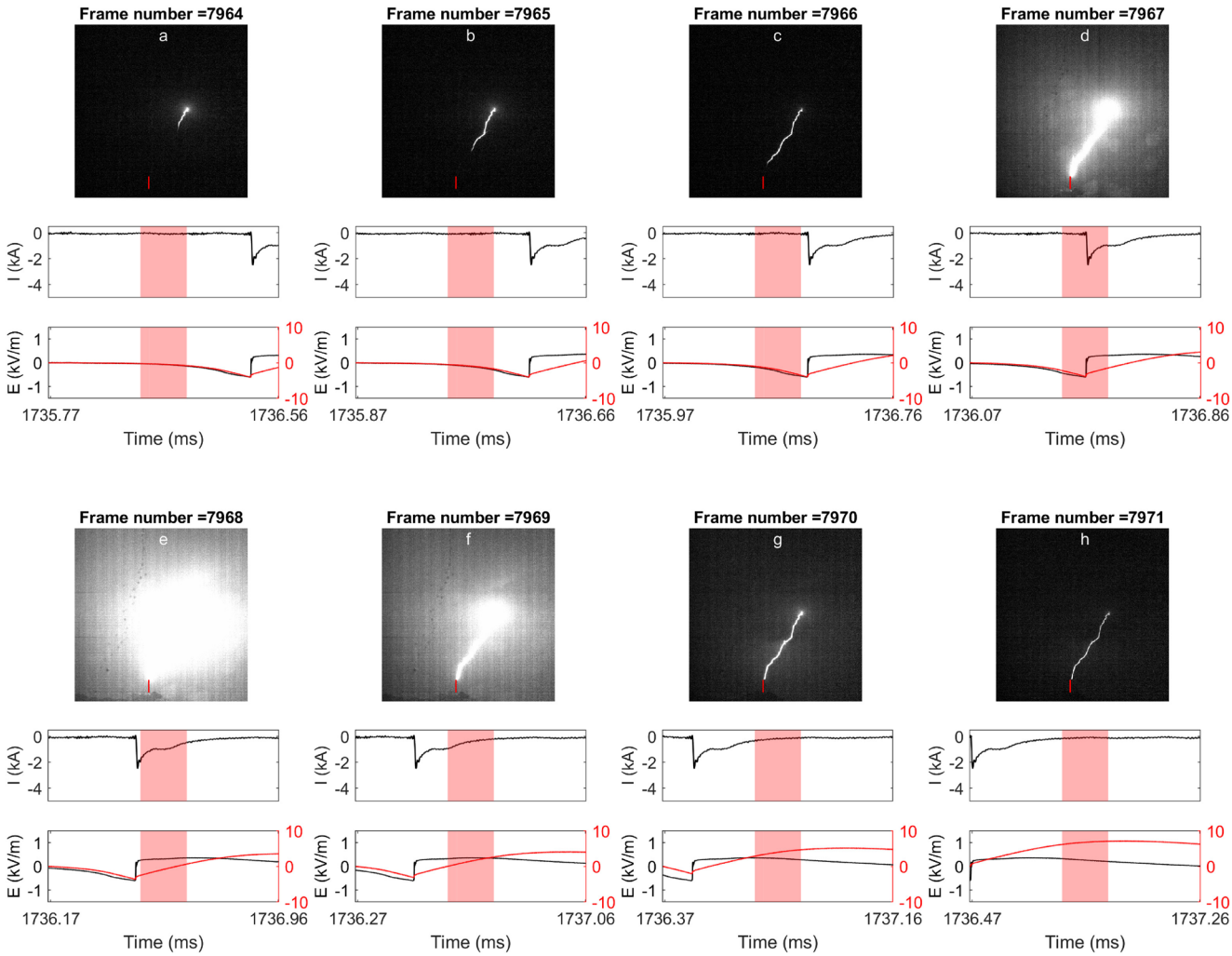

Figure 10. First return stroke (RS) event. See description of subplots in the captions of Figures 3 and 7.

4.4. Comparison of the Recoil Leader Luminosity Brightness in Different Phenomena

In Figure 12, we present the average luminosity brightness per unit length of all RLs for the observed ALs, M-ICC events and RSs. We can observe that M-ICC events and RSs are initiated by bright RLs. One of the M-ICC RLs had a relatively low luminosity. However, in this case, we had two RLs at the same time as can be seen in Figure 7c. We could expect brighter RLs to be initiated in the case of a stronger electric field. It is reasonable to assume that a stronger field would also result in a longer RL and, therefore, a higher probability of reaching the ground. A strong field could also initiate more than one RL at the same time, as in the case of Figure 7c.

5. Bidirectional Recoil Leader Propagation

We have not observed any bidirectional propagation in the analyzed RLs of Flash #3. This can be explained by the fact that our FPS rate (10 k) was smaller than that of Mazur et al. (2013) (54 k). In most cases, we had only one frame for the whole RL. Even in the cases for which we did have more than one frame, it is also possible that the positive end was no longer propagating after the first frame. It was indeed observed in Mazur et al. (2013) (see Figure 4) and (Wu et al., 2019) that, in the beginning, the positive end was propagating slower than the negative, and after some time, the positive leader seems to cease to propagate.

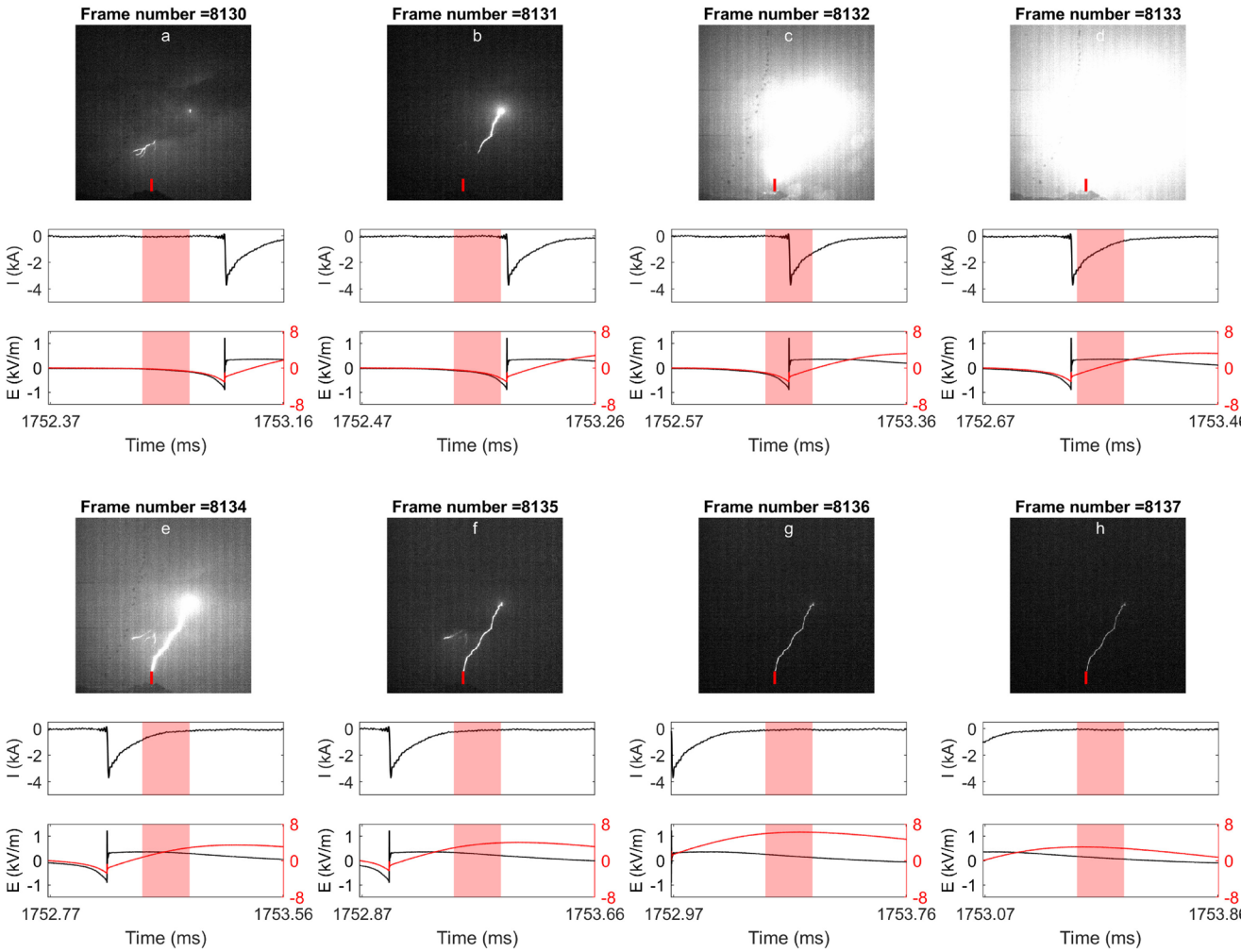

Figure 11. Second return stroke (RS) event. See description of subplots in the captions of Figures 3 and 7.

However, we have observed bidirectional propagation in three RLs belonging to Flash #2: one AL and two RSs (see Figure 13). Figure 14 presents the bidirectional propagation in an AL that occurred along the decayed ICC channel. We can observe bidirectional propagation from Figure 14b to Figure 14c.

Figure 15 and Figure 16 present the observations associated with the two RSs belonging to Flash #2, for which we can observe bidirectional propagation of the RL in Figure 15b to 15c and Figures 16b to 16c. It can be seen that in later stages (Figures 15c to 15d and Figures 16c to 16d), the positive end is no longer observed to propagate, presumably because either it was obscured by the clouds, or the critical electric field condition was no longer satisfied. This fact could explain why in some cases with a limited number of frames, we were not able to confirm a bidirectional propagation as the positive end could have ceased to propagate already by the end of the exposure time of the first observed frame.

6. Discussion

HSC observations of different processes, namely RSs, M-ICC events, and ALs, characterized by different current and electric field waveforms were discussed. The observations show that all these processes start as RLs, based on the fact that they propagate with speeds characteristic of DLs and they propagate along a decayed channel as observed from HSC video. It is worth noting that in our observations, RLs always start at the extremity of decayed channels. Although we did not observe any M components or MM pulses in the flash that was analyzed in detail, we did observe them in the two other flashes, which are presented in

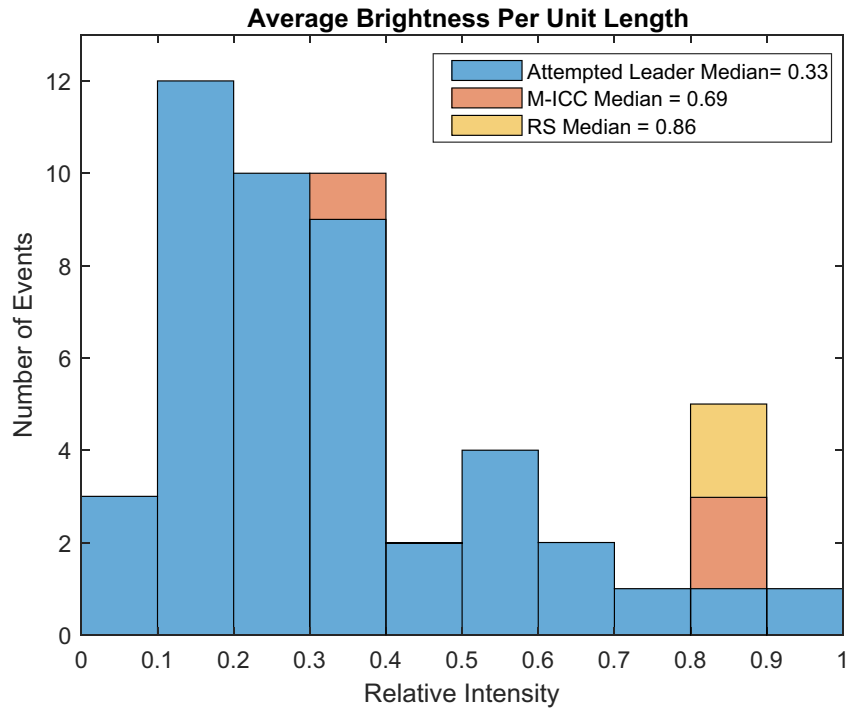

Figure 12. Histogram of the average luminosity brightness per unit length for recoil leaders (RLs) resulting in different phenomena.

the supplementary material (Sunjerga, Rachidi, & Rubinstein, 2021). Both M components and MM pulses propagated with speeds characteristic of DLs and not those of dart stepped leaders (that develop along previously created but decayed channels), suggesting that they are also originating from RLs propagating along ionized paths.

An illustrated summary of the observations presented in this work is shown in Figure 17. Note that we assume that the negative part of the RL is longer (see [Sunjerga, Rubinstein, et al., 2021] for more details) than the positive part, and that the positive end stops to extend at a certain point (see [Mazur et al., 2013]). The figure can be described as follows.

In our observations, all the processes start with a RL. Note that this might be partially due to the fact that the camera view was concentrated in proximity of the tower tip and there might be part of a recoil leader out

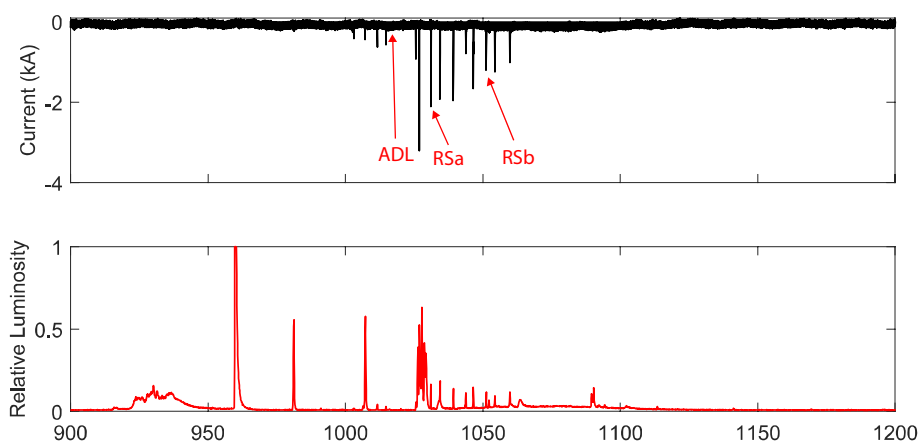

Figure 13. Current and relative luminosity for Flash #2. Bidirectional recoil leaders (RLs) were observed with an attempted leader (AL) and two return strokes (RSs) marked in the figure.

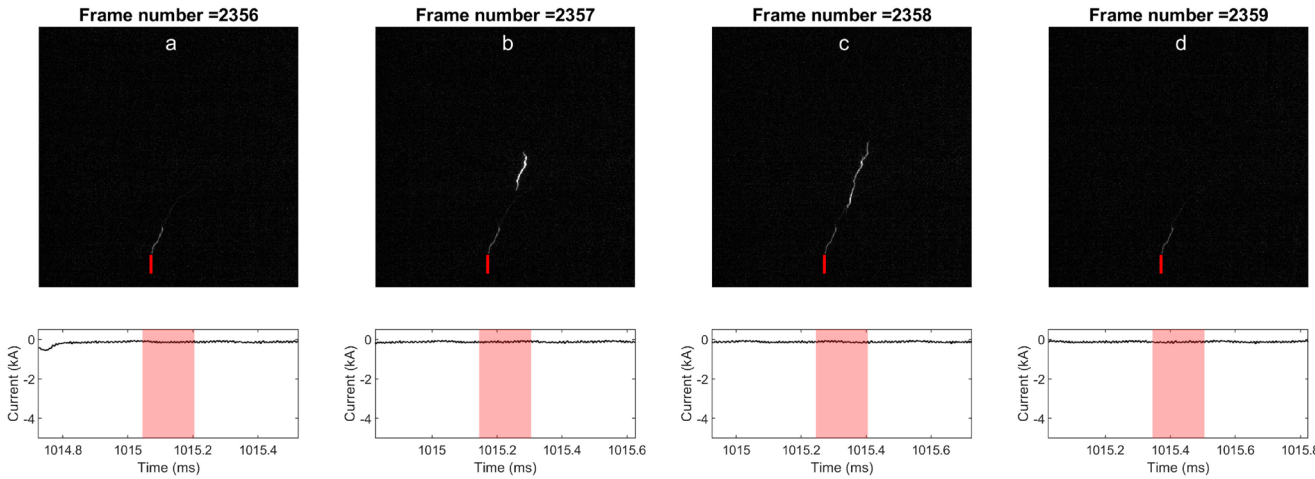

Figure 14. Attempted leader (AL) in Flash #2 with bidirectional propagation of the recoil leader (RL). Frames from the high-speed camera (HSC) are shown on the top and the corresponding current waveform on the bottom. The red shaded time intervals in the field plots are 160 μs wide and they represent a 99 μs exposure of each frame and an extra 61 μs estimated uncertainty due to the manual time synchronization.

of the view propagating as virgin air breakdown and extending the channel. A DL is created when the RL or virgin air breakdown retraces the old channel and reaches either (a) the ground (or the tip of the tower), resulting in a subsequent stroke or a MM pulse, or (b) a conducting channel, resulting in an M-component or an M-ICC pulse. What follows after will depend on the type of junction (to the structure or to a conducting channel) and the presence of another conducting branch. This confirms once again (Shao et al., 1995; and Mazur, 2002) that a RL is the main cause for the sequence of different events observed in upward and downward negative lightning.

7. Conclusion

We analyzed three upward negative flashes at the Säntis Tower using a high-speed video camera. The channel-base lightning current was also observed using direct measurements on the tower. In one of the flashes, simultaneous records of electric fields at 23 m distance were also obtained. A detailed analysis of this flash was presented in the paper. During the flash, 50 recoil leaders were observed, 45 of which ended up as attempted leaders, three developed into M-component-type ICC processes, and two into return strokes.

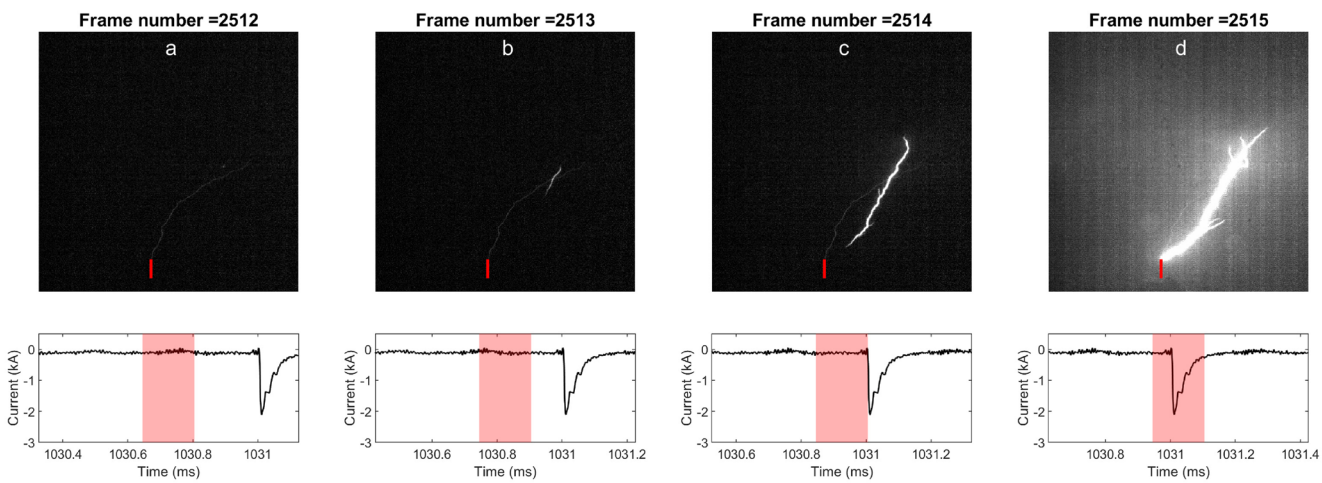

Figure 15. Return stroke (RS) *a* from Flash #2 with bidirectional propagation of the recoil leader (RL). The description is the same as in Figure 14.

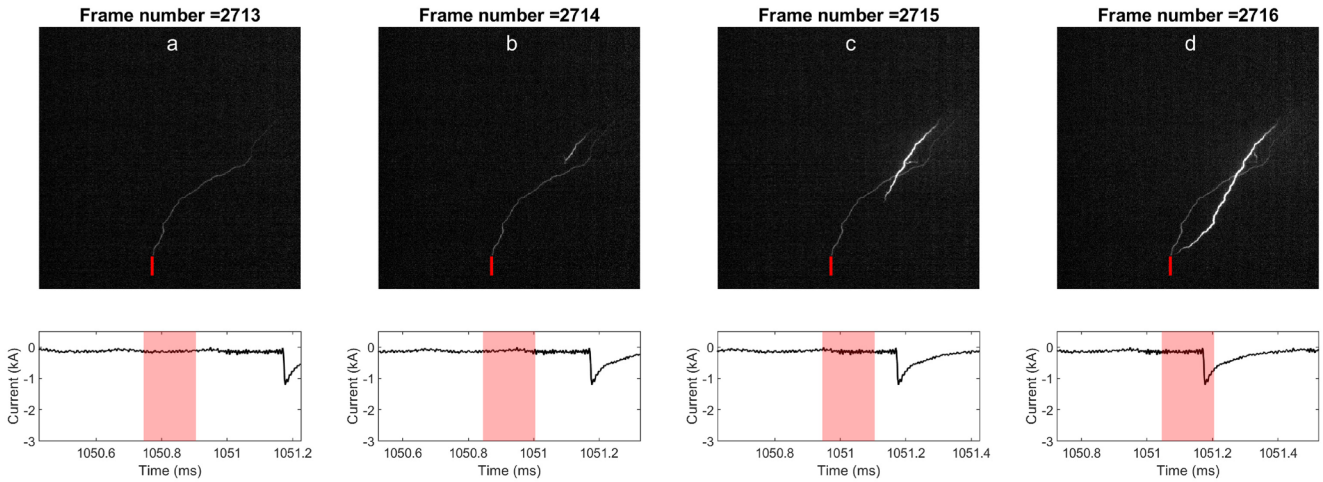

Figure 16. Return stroke (RS) *b* from Flash #2 with bidirectional propagation of the recoil leader (RL). The description is the same as in Figure 14.

We observed that different processes occurring in upward negative flashes, including the return stroke, mixed-mode pulses, M-components, M-component-type ICC events, and attempted leaders all started as recoil leaders. Depending on the spatial and temporal properties of the electric field in the area of the event and the main channel condition, the recoil leader can develop into one of these phenomena.

Our observations suggest that mixed-mode pulses occur only when the dart leader connects directly to the structure, while junction to the conducting channel at any height will cause M-component-type ICC pulses.

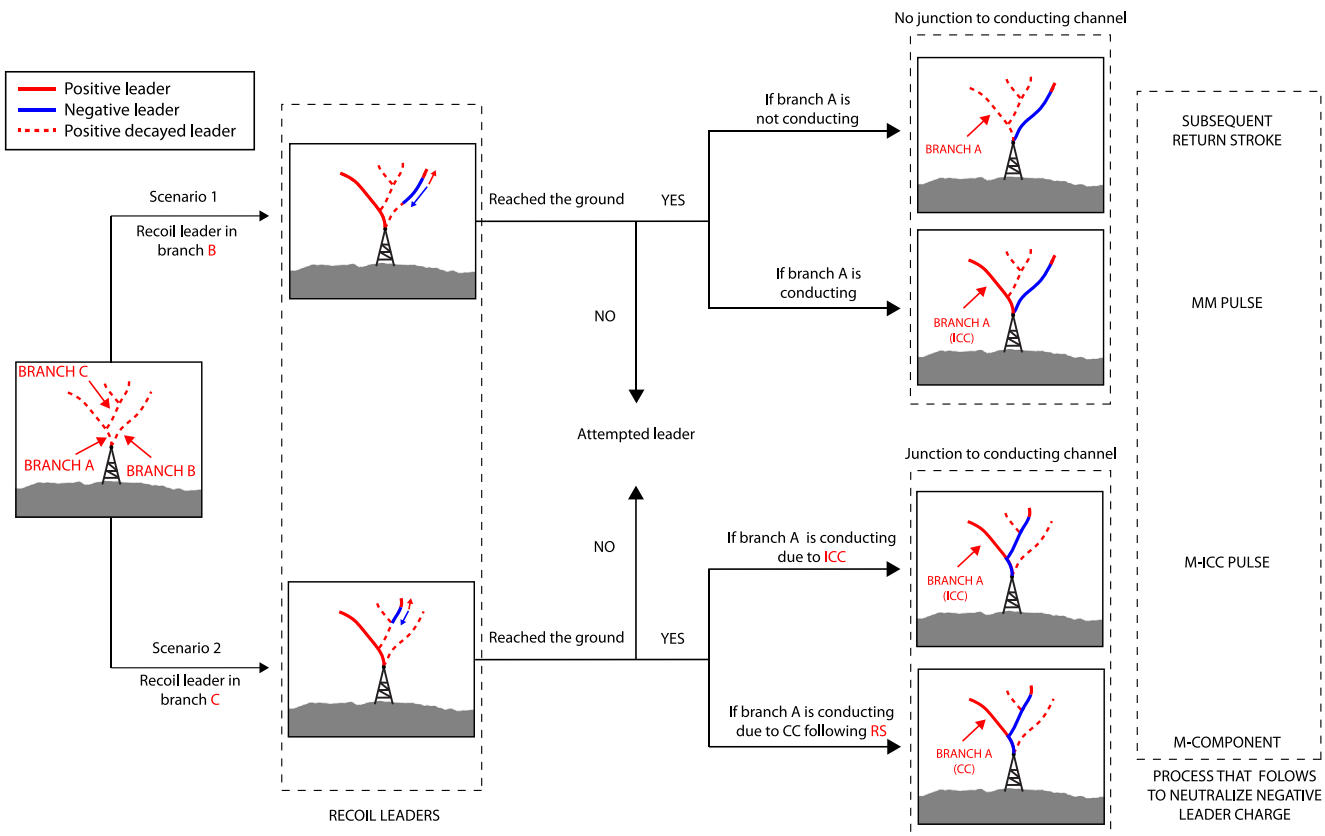

Figure 17. Sketch of mechanisms involved in the initiation of different charge transfer modes in upward negative flashes, all of them starting from recoil leaders (RLs), as observed at Säntis. Not to scale.

Furthermore, our observations suggest that not only return strokes and mixed-mode pulses consist of the dart leader/return stroke phase. A similar phase can be also observed in M-components and M-component-type ICC events in parts of channel above the junction point.

All the observed M-component-type ICC events connected to the channel at a relatively low altitude of a few hundred meters, providing evidence that the junction points of M-component-type ICC events can be significantly lower than the 1-km threshold suggested earlier in literature (Zhou et al., 2015).

Bidirectional propagation of recoil leaders was also observed in three recoil leaders leading to an attempted leader and in two return strokes. Observations suggest that in later stages of the recoil leader development, the positive end ceases to propagate.

Data Availability Statement

Supplementary data are available at Sunjerga, Rachidi, & Rubinstein, 2021.

Acknowledgments
This work was supported in part by the Swiss National Science Foundation (Project No. 200020_175594). Open access funding enabled and organized by Projekt DEAL.

References

Azadifar, M., Paolone, M., Pavanello, D., Rachidi, F., Romero, C., & Rubinstein, M. (2014). "An update on the instrumentation of the Säntis Tower in Switzerland for lightning current measurements and obtained results". In CIGRE international colloquium on lightning and power systems.

Azadifar, M., Rachidi, F., Rubinstein, M., Rakov, V. A., Paolone, M., Pavanello, D., & Metz, S. (2016). Fast initial continuous current pulses versus return stroke pulses in tower-initiated lightning. *Journal of Geophysical Research: Atmospheres*, *121*(11), 6425–6434. https://doi.org/10.1002/2016jd024900

Azadifar, M., Rubinstein, M., Li, Q., Rachidi, F., & Rakov, V. (2019). A New Engineering Model of Lightning M Component That Reproduces Its Electric Field Waveforms at Both Close and Far Distances. *Journal of Geophysical Research: Atmospheres*, *124*(24), 14008–14023. https://doi.org/10.1029/2019jd030796

Cooray, G. V. (2014). *The lightning flash IEE, power & energy series* (2nd ed.).

Cooray, V., Rubinstein, M., & Rachidi, F. (2020). Latitude and topographical dependence of lightning return stroke peak current in natural and tower-initiated negative ground flashes. *Atmosphere*, *11*(6), 560. https://doi.org/10.3390/atmos11060560

Diendorfer, G., Pichler, H., & Mair, M. (2009). Some parameters of negative upward-initiated lightning to the Gaisberg Tower (2000–2007). *IEEE Transactions on Electromagnetic Compatibility*, *51*, 443–452. https://doi.org/10.1109/temc.2009.2021616

He, L., Azadifar, M., Rachidi, F., Rubinstein, M., Rakov, V. A., Cooray, V., et al. (2018). An analysis of current and electric field pulses associated with upward negative lightning flashes initiated from the Säntis Tower. *Journal of Geophysical Research: Atmospheres*, *123*(8), 4045–4059. https://doi.org/10.1029/2018jd028295

Heidler, F. H., Manhardt, M., & Stimper, K. (2013). The slow-varying electric field of negative upward lightning initiated by the Peissenberg Tower, Germany. *IEEE Transactions on Electromagnetic Compatibility*, *55*(2), 353–361. https://doi.org/10.1109/temc.2012.2209121

Hussein, A. M., Janischewskyj, W., Chang, J.-S., Shostak, V., Chisholm, W. A., Dzurevych, P., & Kawasaki, Z.-I. (1995). Simultaneous measurement of lightning parameters for strokes to the Toronto Canadian National Tower. *Journal of Geophysical Research*, *100*(D5), 8853. https://doi.org/10.1029/95jd00543

Jiang, R., Wu, Z., Qie, X., Wang, D., & Liu, M. (2014). High-speed video evidence of a dart leader with bidirectional development. *Geophysical Research Letters*, *41*(14), 5246–5250. https://doi.org/10.1002/2014gl060585

Kasemir, H. W. (1950). Qualitative ubersicht uber potential-, feld- und ladungsverhaltnisse bei einer blitzentladung inder gewitterwolke (qualitative survey of the potential, field and charge conditions during a lightning dischargein the thunderstorm cloud). In H. Israel (Ed.), *Das Gewitter*. Leipzig: Akadem. Verlagsgesellschaft.

Kitagawa, N., & Brook, M. (1960). A comparison of intracloud and cloud-to-ground lightning discharges. *Journal of Geophysical Research*, *65*(4), 1189–1201. https://doi.org/10.1029/jz065i004p01189

Kotovsky, D. A., Uman, M. A., Wilkes, R. A., & Jordan, D. M. (2019). High-speed video and lightning mapping array observations of incloud lightning leaders and an M component to ground. *Journal of Geophysical Research: Atmospheres*, *124*(3), 1496–1513. https://doi.org/10.1029/2018jd029506

Krehbiel, P. R., Brook, M., & McCrory, R. A. (1979). An analysis of the charge structure of lightning discharges to ground. *Journal of Geophysical Research*, *84*(C5), 2432. https://doi.org/10.1029/jc084ic05p02432

Li, D., Azadifar, M., Rachidi, F., Rubinstein, M., Paolone, M., Pavanello, D., et al. (2016). On lightning electromagnetic field propagation along an irregular terrain. *IEEE Transactions on Electromagnetic Compatibility*, *58*(1), 161–171. https://doi.org/10.1109/temc.2015.2483018

Mazur, V. (2002). Physical processes during development of lightning flashes. *Comptes Rendus Physique*, *3*(10), 1393–1409. https://doi.org/10.1016/s1631-0705(02)01412-3

Mazur, V., & Ruhnke, L. H. (1993). Common physical processes in natural and artificially triggered lightning. *Journal of Geophysical Research*, *98*(D7), 12913. https://doi.org/10.1029/93jd00626

Mazur, V., & Ruhnke, L. H. (2011). Physical processes during development of upward leaders from tall structures. *Journal of Electrostatics*, *69*(2), 97–110. https://doi.org/10.1016/j.elstat.2011.01.003

Mazur, V., Ruhnke, L. H., Warner, T. A., & Orville, R. E. (2013). RL formation and development. *Journal of Electrostatics*, *71*(4), 763–768. https://doi.org/10.1016/j.elstat.2013.05.001

Qie, X., Pu, Y., Jiang, R., Sun, Z., Liu, M., Zhang, H., et al. (2017). Bidirectional leader development in a preexisting channel as observed in rocket-triggered lightning flashes. *Journal of Geophysical Research: Atmospheres*, *122*(2), 586–599. https://doi.org/10.1002/2016jd025224

Romero, C., Mediano, A., Rubinstein, A., Rachidi, F., Rubinstein, M., Paolone, M., et al. (2010). Measurement of lightning currents using a combination of Rogowski coils and B-dot sensors. *2010 30th international conference on lightning protection (ICLP)*. https://doi.org/10.1109/iclp.2010.7845959

Romero, C., Paolone, M., Rubinstein, M., Rachidi, F., Rubinstein, A., Diendorfer, G., et al. (2012). A system for the measurements of lightning currents at the Säntis Tower. *Electric Power Systems Research*, *82*(1), 34–43. https://doi.org/10.1016/j.epsr.2011.08.011

Romero, C., Rachidi, F., Paolone, M., & Rubinstein, M. (2013). Statistical distributions of lightning currents associated with upward negative flashes based on the data collected at the Säntis Tower in 2010 and 2011. *IEEE Transactions on Power Delivery*, *28*(3), 1804–1812. https://doi.org/10.1109/tpwrd.2013.2254727

Rubenstein, M., Rachidi, F., Uman, M. A., Thottappillil, R., Rakov, V. A., & Nucci, C. A. (1995). Characterization of vertical electric fields 500 m and 30 m from triggered lightning. *Journal of Geophysical Research*, *100*(D5), 8863. https://doi.org/10.1029/95jd00213

Rubinstein, M., Bermdez, J., Rakov, V., Rachidi, F., & Hussein, A. (2012). Compensation of the instrumental decay in measured lightning electric field waveforms. *IEEE Transactions on Electromagnetic Compatibility*, *54*(3), 685–688. https://doi.org/10.1109/temc.2012.2198482

Saba, M. M. F., Cummins, K. L., Warner, T. A., Krider, E. P., Campos, L. Z. S., Ballarotti, M. G., et al. (2008). Positive leader characteristics from high-speed video observations. *Geophysical Research Letters*, *35*(7). https://doi.org/10.1029/2007gl033000

Shao, X. M., Krehbiel, P. R., Thomas, R. J., & Rison, W. (1995). Radio interferometric observations of cloud-to-ground lightning phenomena in Florida. *Journal of Geophysical Research*, *100*(D2), 2749. https://doi.org/10.1029/94jd01943

Shindo, T., Miki, T., Saito, M., Tanaka, D., Asakawa, A., Motoyama, H., et al. (2014). Lightning observations at Tokyo Skytree. In *2014 international symposium on electromagnetic compatibility - EMC EUROPE*. https://doi.org/10.1109/emceurope.2014.6930973

Smorgonskiy, A., Egüz, E., Rachidi, F., Rubinstein, M., & Cooray, V. (2015). A model for the evaluation of the electric field associated with the lightning-triggering rocket wire and its corona. *Journal of Geophysical Research: Atmospheres*, *120*(20), 10964–10973. https://doi.org/10.1002/2015jd023373

Sunjerga, A., Rachidi, F., & Rubinstein, M. (2021). *Bidirectional recoil leaders in upward lightning flashes observed at the Säntis Tower.zip*. figshare. Dataset. https://doi.org/10.6084/m9.figshare.14588346.v2

Sunjerga, A., Rubinstein, M., Pineda, N., Mostajabi, A., Azadifar, M., Romero, D., & Rachidi, F. (2020). LMA observations of upward lightning flashes at the Säntis Tower initiated by nearby lightning activity. *Electric Power Systems Research*, *181*, 106067. https://doi.org/10.1016/j.epsr.2019.106067

Sunjerga, A., Rubinstein, M., Rachidi, F., & Cooray, V. (2021). On the initiation of upward negative lightning by nearby lightning activity: An analytical approach. *Journal of Geophysical Research: Atmospheres*, *126*. https://doi.org/10.1029/2020jd034043

Warner, T. A., Cummins, K. L., & Orville, R. E. (2012). Upward lightning observations from towers in Rapid City, South Dakota and comparison with National Lightning Detection Network data, 2004-2010. *Journal of Geophysical Research*, *117*(D19). https://doi.org/10.1029/2012jd018346

Warner, T. A., Saba, M. M. F., Schumann, C., Helsdon, J. H., Jr, & Orville, R. E. (2016). Observations of bidirectional lightning leader initiation and development near positive leader channels. *Journal of Geophysical Research: Atmospheres*, *121*(15), 9251–9260. https://doi.org/10.1002/2016jd025365

Wu, B., Lyu, W., Qi, Q., Ma, Y., Chen, L., Jiang, R., et al. (2019). High-speed video observations of recoil leaders producing and not producing return strokes in a Canton-Tower upward flash. *Geophysical Research Letters*, *46*(14), 8546–8553. https://doi.org/10.1029/2019gl083862

Yoshida, S., Biagi, C. J., Rakov, V. A., Hill, J. D., Stapleton, M. V., Jordan, D. M., et al. (2012). The initial stage processes of rocket-and-wire triggered lightning as observed by VHF interferometry. *Journal of Geophysical Research*, *117*(D9). https://doi.org/10.1029/2012jd017657

Zhou, H., Rakov, V. A., Diendorfer, G., Thottappillil, R., Pichler, H., & Mair, M. (2015). A study of different modes of charge transfer to ground in upward lightning. *Journal of Atmospheric and Solar-Terrestrial Physics*, *125–126*, 38–49. https://doi.org/10.1016/j.jastp.2015.02.008

Zhu, Y., Ding, Z., Rakov, V. A., & Tran, M. D. (2019). Evolution of an upward negative lightning flash triggered by a distant +cg from a 257-m-tall tower, including initiation of subsequent strokes. *Geophysical Research Letters*, *46*(12), 7015–7023. https://doi.org/10.1029/2019gl083274